

Wind-Driven Atlantic Water Flow as a Direct Mode for Reduced Barents Sea Ice Cover

VIDAR S. LIEN

Institute of Marine Research, Bergen, Norway

PAWEL SCHLICHTHOLZ

Institute of Oceanology, Polish Academy of Sciences, Sopot, Poland

ØYSTEIN SKAGSETH AND FRODE B. VIKEBØ

Institute of Marine Research, and Bjerknes Centre for Climate Research, Bergen, Norway

(Manuscript received 23 December 2015, in final form 7 October 2016)

ABSTRACT


Variability in the Barents Sea ice cover on interannual and longer time scales has previously been shown to be governed by oceanic heat transport. Based on analysis of observations and results from an ocean circulation model during an event of reduced sea ice cover in the northeastern Barents Sea in winter 1993, it is shown that the ocean also plays a direct role within seasons. Positive wind stress curl and associated Ekman divergence causes a coherent increase in the Atlantic water transport along the negative thermal gradient through the Barents Sea. The immediate response connected to the associated local winds in the northeastern Barents Sea is a decrease in the sea ice cover due to advection. Despite a subsequent anomalous ocean-to-air heat loss on the order of 100 W m^{-2} due to the open water, the increase in the ocean heat content caused by the circulation anomaly reduced refreezing on a time scale of order one month. Furthermore, it is found that coherent ocean heat transport anomalies occurred more frequently in the latter part of the last five decades during periods of positive North Atlantic Oscillation index, coinciding with the Barents Sea winter sea ice cover decline from the 1990s and onward.

1. Introduction

During the last few decades, the Arctic has experienced large climatic changes, manifested by its shrinking sea ice cover (Polyakov et al. 2010). While the most spectacular decline during summer has occurred on the Pacific side of the Arctic, the largest variability and decline in winter has occurred on the Atlantic side in the Barents Sea (Johannessen et al. 2004; Screen and Simmonds 2010; Onarheim et al. 2015; Yang et al. 2016). The diminishing ice cover and the associated impacts have deservedly received a lot of attention (e.g., Serreze et al. 2007; Comiso 2012; Parkinson and Cavalieri 2012). Variable air–sea heat fluxes caused by a changing sea ice cover may

act as important drivers of large-scale atmospheric circulation variability (Screen et al. 2013; Frankignoul et al. 2014; Cohen et al. 2014) and have been considered a cause for the midlatitude cold winters in recent years (e.g., Petoukhov and Semenov 2010; Vihma 2014; Cohen et al. 2014; Mori et al. 2014) and changes to the circulation in the upper troposphere (Schlichtholz 2014); they have been connected to surface temperature in midlatitudes (Schlichtholz 2016), although the causal relationship is complex (Sorokina et al. 2016). Changes in the sea ice cover also impact regional marine resources and ecosystems, including species distributions, abundances, and interactions (Fossheim et al. 2015); availability of light (Varpe et al. 2015); and commercial offshore activity, such as shipping and fossil fuel extraction [e.g., Arctic Climate Impact Assessment (ACIA 2005)].

The Barents Sea is a shelf sea between the deep Norwegian Sea and Arctic Ocean basins. The hydrography in the Barents Sea is dominated by relatively

 Denotes Open Access content.

Corresponding author e-mail: Vidar S. Lien, vidar.lien@imr.no

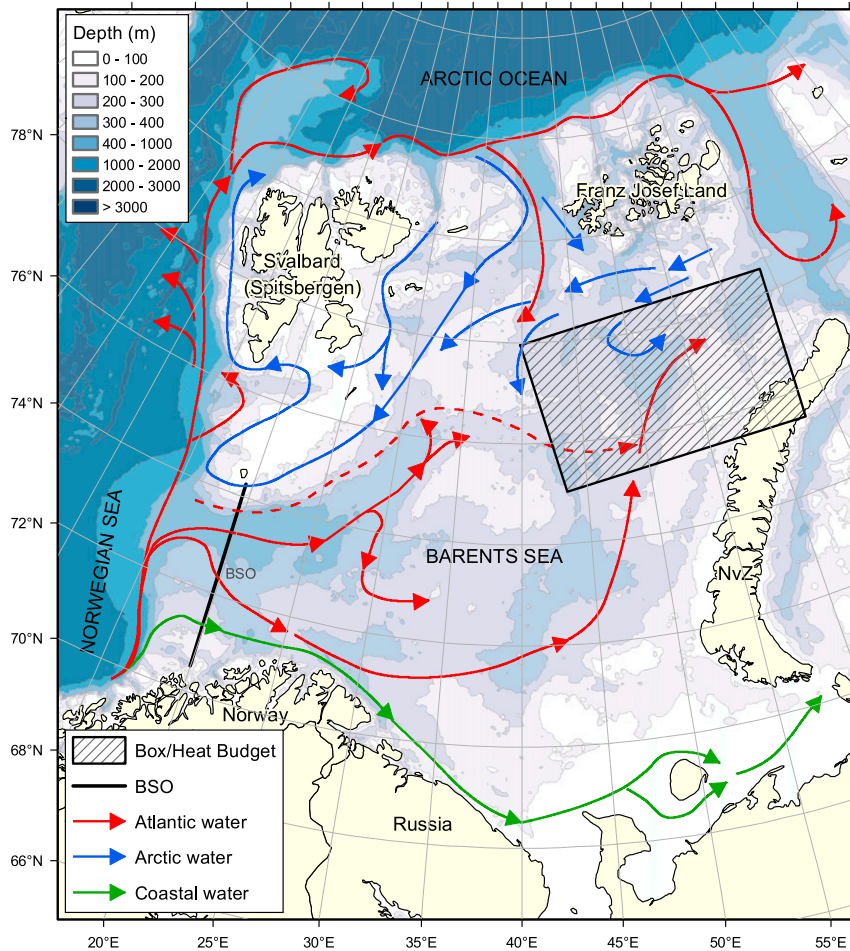


FIG. 1. Map showing the bathymetry and general circulation pattern of the Barents Sea. Black line shows the position of the section across the Barents Sea Opening; shaded area shows the box in the northeastern Barents Sea used in budget calculations; NvZ denotes Novaya Zemlya. The whole area depicted is included within the model domain.

warm and saline Atlantic-derived water masses and cold and less saline Arctic-derived water masses. The Atlantic water enters from the Norwegian Sea in the southwest and is topographically steered toward the northeast (Fig. 1). In the northern parts, the Arctic-derived water masses dominate, although some Atlantic water enters from the north at depths below 100 m (Lind and Ingvaldsen 2012). The shallow, southeastern parts are dominated by coastal water freshened by river runoff. The sea ice extent in winter is partly determined by the transition zone between the Atlantic and Arctic water masses, often termed the Polar Front. To the southeast, the ice extent is determined by the frontal area between Atlantic and coastal waters. The Polar Front is topographically controlled and therefore rather stable in the west, where the thermal gradient is oriented perpendicular to the direction of the flow. To the northeast, the thermal gradient is oriented along the flow of Atlantic

water because of heat loss to the atmosphere. Hence, a positive volume transport anomaly will cause a coherent temperature increase rather than an advectively propagating temperature anomaly (Sundby and Drinkwater 2007; Chafik et al. 2015). The northeastern Barents Sea is the area where the winter sea ice extent displays the largest variability (Årthun et al. 2012; Yang et al. 2016).

Previous studies on the air–ice–ocean relationship in the Barents Sea have been based on correlation and lead–lag analyses, pointing to a lagged response of sea ice to upstream advective ocean temperature anomalies. However, the mechanisms governing the response in the sea ice cover to oceanic and atmospheric forcing are not yet fully understood. The time lag between the inflow of ocean temperature anomalies through the Barents Sea Opening in the southwest and the associated changes in sea ice cover downstream is reported to be between one month (e.g., Sandø et al. 2010) and one

year (e.g., Schlichtholz 2011; Årthun et al. 2012; Onarheim et al. 2015). A one-year time lag is consistent with an advection speed of less than 5 cm s^{-1} , similar to the observed current speeds in the Barents Sea Opening (Ingvaldsen et al. 2002), and involves subsurface advection of the ocean temperature anomalies below the seasonally modified surface water masses and a subsequent reemergence downstream (Schlichtholz 2011; Nakanowatari et al. 2014). The one-month time lag reported by Sandø et al. (2010) was based on 12-month smoothed data and was therefore difficult to interpret, and they did not explore any possible mechanism. Other studies argue for a close coupling between the variability in the sea ice cover and the properties of the Atlantic water and the atmospheric circulation, but without studying the mechanisms in detail (Ozhigin et al. 2011; Smedsrud et al. 2013). Variations in sea ice cover on short time scales (i.e., days to weeks) have been attributed to wind-driven ice drift (e.g., Kimura and Wakatsuchi 2001), although atmospheric forcing has also been shown to affect sea ice cover on longer and up to interannual time scales (Sorteberg and Kvingedal 2006; Pavlova et al. 2014; Herbaut et al. 2015).

A critical assumption in the understanding of the Barents Sea air–ice–ocean relationship is that ocean temperature anomalies propagate from an upstream formation area to the ice edge downstream. Here, we provide a mechanistic understanding of the response of sea ice to ocean heat anomalies modulated by changes in volume transport. Continental shelf waves induced by atmospheric-driven Ekman transports and the piling up of water toward the coast of Norway (Gill and Schumann 1974; Ingvaldsen et al. 2004; Skagseth et al. 2011; Lien et al. 2013a) are shown to result in a coherent ocean heat transport anomaly through the Barents Sea that impacts the sea ice cover concomitantly. We combine observations and a numerical ocean general circulation model to study in detail a period of increased Atlantic water flow through the Barents Sea in February 1993 and quantify the relationship between this increased oceanic heat transport and a simultaneous reduction in the sea ice cover. Furthermore, we find that similar oceanic conditions occurred more frequently in the latter part of the last five decades during periods of positive North Atlantic Oscillation index (NAO; Hurrell 1995).

2. Data

a. Atmosphere

Air–ocean heat fluxes, including longwave and shortwave radiation and turbulent latent and sensible heat, and wind stress data for the period 1979–2014 were obtained

from the European Centre for Medium-Range Weather Forecasts interim reanalysis (ERA-Interim; Dee et al. 2011). Acknowledging that most atmospheric reanalyses, such as ERA-Interim, use parameterized algorithms based on typical conditions at lower latitudes, we assume that temporal variability is still reasonably well represented at high latitudes, such as the Barents Sea. See Smedsrud et al. (2013) for a discussion on the differences between various datasets containing atmospheric heat fluxes in the Barents Sea. Additional wind stress data extending back to 1979 were obtained from the NCEP–NCAR reanalysis (Kalnay et al. 1996).

b. Sea ice

Monthly averaged sea ice concentrations (Fig. 2) for the period 1979–2014 were obtained from National Snow and Ice Data Center (NSIDC), Boulder, Colorado (Cavalieri et al. 1996). The NSIDC web page (www.nsidc.org/data/NSIDC-0051) states that care is needed when interpreting the observations of sea ice concentration in areas where new sea ice makes up a substantial part of the sea ice cover, which include our area of study during winter. Our interpretation of the sea ice concentration data from the northeastern Barents Sea is based on the assumption that errors related to issues with newly formed sea ice are constant in time: that is, that the observed temporal variability of sea ice concentration can be considered to be valid. The monthly mean sea ice data were deseasoned and detrended by removing the 1979–2014 seasonal cycle and linear trend before calculating anomalies.

c. Ocean model

We utilize the Regional Ocean Modeling System (ROMS; Shchepetkin and McWilliams 2005), a three-dimensional baroclinic ocean general circulation model that uses topography-following s coordinates in the vertical. The s coordinates map all 32 model layers in all grid points independent of the bottom depth, which ensures high vertical resolution in shelf areas such as the Barents Sea. The model simulation was performed on an orthogonal, curvilinear grid with a horizontal resolution of 4 km covering the Nordic, Barents, and Kara Seas plus the Nansen Basin of the Arctic Ocean. In the vertical we applied 32 sigma layers with a minimum depth of 10 m. The modeled period is 1958–2014, starting from an already spun-up initial condition in 1958. However, the first two years have been discarded as model spinup.

We have used a 10-km-resolution atmospheric reanalysis for the Nordic seas area as forcing (Reistad et al. 2011). The Simple Ocean Data Assimilation, version 2.1.6, reanalysis (SODA 2.1.6; Carton et al. 2000; Carton and Giese 2008) was used both for initialization

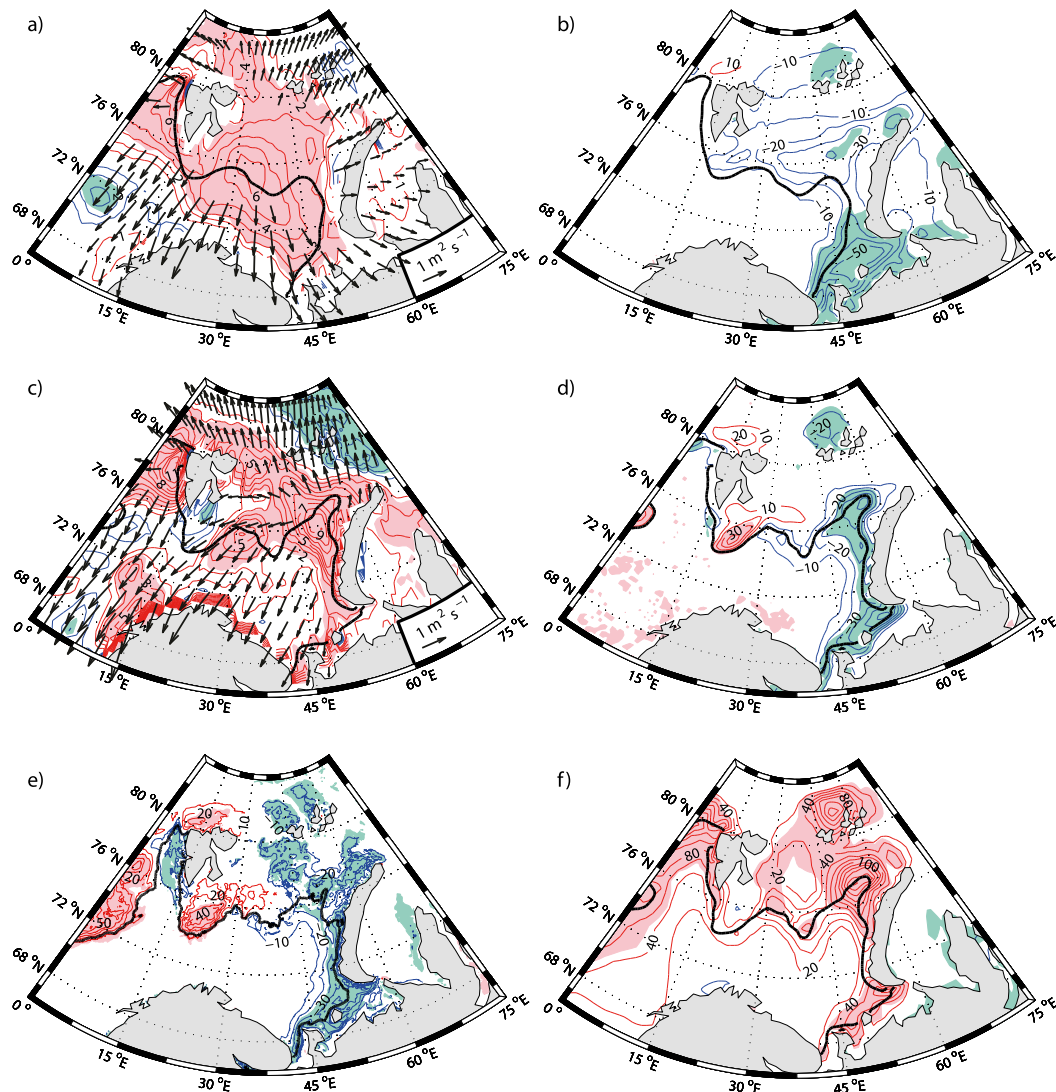


FIG. 2. (a) Difference in wind stress curl (contours; 10^{-7} N m^{-3}) and Ekman transport (arrows; $\text{m}^2 \text{ s}^{-1}$) between Februaries with positive and negative wind stress curl anomalies exceeding one std dev, computed over the entire Barents Sea (66° – 82°N , 15° – 60°E ; land excluded), from ERA-Interim. Red and green contours show positive and negative anomalies, respectively. Shaded areas denote values outside one std dev (corresponding to a confidence level of 68%). Thick black line shows average February ice edge position as defined by 15% sea ice concentration. (b) As in (a), but showing differences in observed sea ice concentration, with the 1979–2014 linear trend removed. Contour interval is 10%. (c) As in (a), but showing anomalies in February 1993, relative to the 1979–2014 February average. Thick black line shows ice edge in February 1993, as defined by 15% sea ice concentration. (d) Observed sea ice concentration anomaly in February 1993, relative to the linearly detrended 1979–2014 February average. Contour interval is 10%. Thick black line shows ice edge in February 1993, as defined by 15% sea ice concentration. (e) As in (d), but based on model results. (f) Observed air–ocean heat (turbulent + radiative) flux anomalies in February 1993, relative to the 1979–2014 February average (W m^{-2} ; positive upward).

and lateral boundary forcing by applying the radiation and nudging boundary conditions scheme by Marchesiello et al. (2001). The nudging time scales are 0.25 days and 25 days for incoming and outgoing information, respectively. The model includes a dynamic–thermodynamic sea ice module based upon an elastic–viscous–plastic rheology (Hunke and Dukowicz 1997; Hunke 2001). The ice

thermodynamics are based on those of Mellor and Kantha (1989) and Häkkinen and Mellor (1992). The ice module includes two ice layers and one snow layer. The ice cover and upper ocean are separated by a molecular sublayer (Mellor et al. 1986). For more details on the sea ice module, see Budgell (2005). Initial and boundary conditions for the sea ice were obtained from a regional simulation using

the Miami Isopycnic Coordinate Ocean Model (MICOM; Sandø et al. 2012). Tidal forcing based on a global ocean tides model (TPXO4) was included by imposing surface elevation and corresponding barotropic velocity components at the open boundaries, as proposed by Flather (1976) and Chapman (1985), respectively. The sea surface salinity was subject to a restoration toward climatological values based on the SODA dataset, with an e -folding time of 180 days.

A third-order upstream scheme was applied for horizontal advection of tracers and momentum. Because of the diffusive nature of this advection scheme, both the explicit horizontal diffusion and viscosity coefficients were set to zero. A nondiffusive fourth-order centered scheme was applied for vertical advection of tracers and momentum. The generic length scale (GLS; Umlauf and Burchard 2003; Umlauf et al. 2003) mixing scheme, using the k - ω setup, was used for subgrid-scale parameterization of vertical turbulent mixing of momentum and tracers. The GLS mixing scheme has been found to produce realistic results in coastal applications where tidal mixing is important (Warner and Geyer 2005; Warner et al. 2005).

The model simulation has been shown to realistically reproduce ocean transports, hydrographic properties, and sea ice cover in the Barents Sea, in terms of both their absolute values and variability (Lien et al. 2013a,b, 2014, 2016; see also Figs. 2d,e herein).

3. Methods

By comparing Februaries with positive and negative wind stress curl anomalies that exceed one standard deviation (Fig. 2a) we find that positive wind stress curl anomalies and associated Ekman divergence calculated from winds coincide with negative anomalies in the sea ice concentration both to the northeast and the southeast in the Barents Sea (Fig. 2b). The pattern of sea ice concentration anomalies corresponding to this anomalous atmospheric circulation resembles that of other studies (e.g., Yang et al. 2016), which suggests that the northeastern Barents Sea is a hotspot for winter sea ice variability, and, because of the presence of Atlantic water, also associated heat flux anomalies (e.g., Sorokina et al. 2016). The choice of one standard deviation in Fig. 2a ensures a reasonable number of events (7 positive and 7 negative out of a total of 35 in the period 1979–2014) and yet retains statistical significance (68%). The results do not differ qualitatively with other choices of significance level. Qualitatively similar results, although with weaker amplitudes, are obtained if we increase or decrease the area used to calculate the average wind stress curl.

TABLE 1. Time and amplitude ($1.0 \times 10^{-6} \text{ N m}^{-3}$) of the nine largest values of the monthly mean wind stress curl averaged over the Barents Sea, based on ERA-Interim (ERA-I) and NCEP. The numbers are sorted in descending order. The area used is 66° – 82° N, 15° – 60° E. Values over land have been excluded.

ERA-I		NCEP	
Time	Amplitude	Time	Amplitude
Jan 1993	0.3503	Feb 1993	0.3887
Feb 1993	0.3459	Jan 1993	0.3395
Jan 1992	0.3422	Jan 2000	0.3370
Jan 2000	0.3199	Jan 1992	0.3297
Dec 1982	0.3095	Jan 1997	0.3072
Feb 1995	0.3038	Nov 1996	0.3024
Nov 1996	0.2949	Feb 1995	0.2953
Nov 1986	0.2752	Dec 1982	0.2950
Dec 2004	0.2714	Dec 2004	0.2858

We investigate in detail processes for the impact of wind-driven ocean circulation on the sea ice cover using the month with the maximum forcing (February 1993; Table 1) as a test case, assuming the best signal-to-noise ratio and under the assumption that the identified mechanism should apply to similar events of atmospheric forcing.

To explore the downstream ocean and ice responses to regional atmospheric forcing, we define a box in the northeastern Barents Sea that covers the Atlantic water pathway through the northeastern Polar Front area where the largest changes in the sea ice cover and ocean-to-air heat fluxes are observed both in terms of decadal trends (Yang et al. 2016; Sorokina et al. 2016) and the February 1993 anomaly (Figs. 2d,f).

The Norwegian Coastal Current responds rapidly to changes in atmospheric forcing (Skagseth et al. 2011). Thus, conditions favorable for increased Atlantic water inflow to the Barents Sea will also favor increased ocean transport along the Norwegian and Russian coast and into the shallow southeastern Barents Sea. While this is associated with a reduction in sea ice (Fig. 2b), the associated turbulent heat flux anomalies are smaller and therefore of limited importance for the Arctic climate (Fig. 2f; see also Sorokina et al. 2016). We therefore focus our study on the Atlantic water pathway through the Barents Sea.

To relate the heat transport estimates to those reported in the literature, the heat transport is calculated with T adjusted by $T_{\text{ref}} = -0.1^{\circ}\text{C}$, commonly referred to as the average temperature of the water masses leaving the Arctic Ocean (Aagaard and Greisman 1975). To resolve the effects of volume transport and temperature on the oceanic heat transport, we decompose the modeled heat transports into mean and fluctuating parts, using 1960–2014 as the averaging period. The calculated heat transport anomaly is then

$$Q' = Q - \rho c_p \bar{T} \bar{V} = \rho c_p (\bar{V} T' + V' \bar{T} + V' T'),$$

where $\rho = 1027.0 \text{ kg m}^{-3}$ is the density of seawater, $c_p = 3985 \text{ J kg}^{-1} \text{ K}^{-1}$ is the specific heat capacity of seawater, T is the temperature ($^{\circ}\text{C}$), and V is the volume transport (Sv ; $1 \text{ Sv} \equiv 10^6 \text{ m}^3 \text{ s}^{-1}$) through the section. The $\bar{T} \bar{V}$ represents the mean seasonal cycle over the period 1960–2014, whereas T' and V' are deviations from the mean. Daily averages of Q' used to study the winter of 1993 in detail have been deseasoned (Fig. 3). Monthly averages of Q used to study the full modeled period (1960–2014; Fig. 5) have been calculated using detrended T .

4. Results

Figure 2c shows the wind stress curl and associated Ekman transport anomalies in February 1993, as compared with the long-term composite of February anomalies (Fig. 2a). Corresponding anomalies in sea ice concentration are shown in Figs. 2d and 2b, respectively. The contributions to the ocean heat transport anomalies through the Barents Sea Opening and into the box in the northeastern Barents Sea are shown in Figs. 3a and 3b, while Fig. 3c shows the energy budget for the box. During January and February 1993, the anomalous atmospheric circulation led to an increase in the heat transport by the Atlantic water flow through the Barents Sea Opening (Fig. 3a). The enhanced heat transport was modulated by an increase in the volume transport [$Q(V', \bar{T})$] and occurred both in the main southern branch of the Barents Sea throughflow and the northern branch, as proposed by Lien et al. (2013a) (indicated by dotted arrow in Fig. 1 herein). The effect of the increased heat transport to the Barents Sea was a simultaneous ocean heat convergence in the box downstream in the northeastern Barents Sea (Fig. 3b), consistent with an atmospheric-driven barotropic ocean circulation anomaly through the Barents Sea (Lien et al. 2013a).

The resulting heat budget for the box additionally considering the contributions of heat exchange with the atmosphere and freezing/melting of sea ice is shown in Fig. 3c. The estimate of the total surface heat flux is obtained by subtracting the contribution from heat storage and ice melting from the net lateral heat convergence. The elevated ocean heat transport anomaly (Figs. 3a,b) was mainly distributed between an initial increase of the ocean heat storage until 1 February and subsequent reduction, and heat loss to the atmosphere reaching a maximum of almost 300 W m^{-2} on 8 February. In addition, there was a relatively small but consistent heat loss of about 20 W m^{-2} from melting sea ice that differed from the climatological mean in February characterized by sea ice freezing.

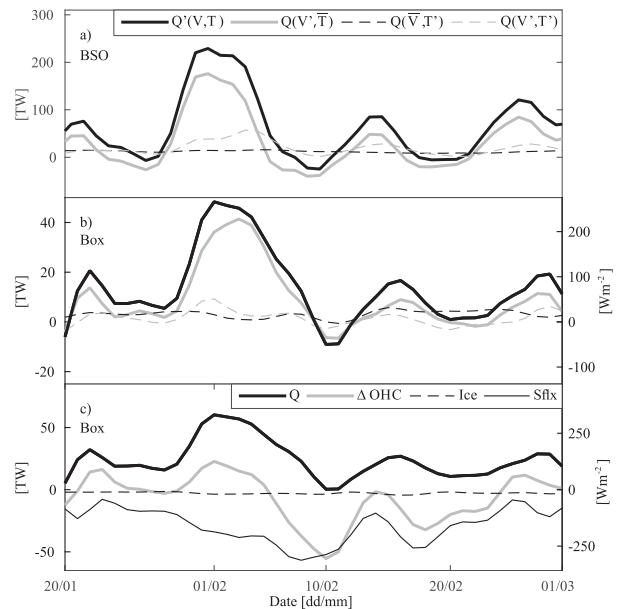


FIG. 3. Modeled heat transport and budget based on daily averages filtered with a 4-day Hamming window. (a) Heat transport anomalies through the Barents Sea Opening section, relative to the 1960–2014 average and $T_{\text{ref}} = -0.1^{\circ}\text{C}$. Positive values are toward the east. Thick black line denotes total anomaly; thick gray line denotes anomaly related to varying volume transport; dashed black line denotes anomaly related to varying temperature; dashed gray line denotes anomaly related to both varying volume transport and temperature. (b) Net lateral heat convergence anomaly in the area denoted by a shaded box in the northeastern Barents Sea (see Fig. 1). The graphs denote the different heat transport components as described in (a). (c) The heat budget components within the box: net lateral heat convergence (Q ; i.e., net ocean heat transport into box area; thick black line); daily change in ocean heat content (ΔOHC ; thick gray line); the heat lost to melting sea ice (Ice; dashed line); and the residual (Sflx; thin black line), which comprises the heat fluxes through the ocean surface as well as diffusive heat advection through lateral boundaries not accounted for in the daily averaged lateral transports. Surface heat flux is counted as negative upward (i.e., heat loss from ocean to atmosphere). Note that (a) and (b) depict anomalies (i.e., deviations from the mean), while (c) shows net values.

To resolve the effect of the ocean circulation anomalies, a comparison with the mean seasonal cycle is required for the ocean heat storage and sea ice terms (Fig. 4). In February 1993, the cumulative change in ocean heat content increased or remained elevated as compared with the long-term seasonal cooling (Fig. 4a). During this period, there was enhanced melting of sea ice from below, amounting to 0.15 m above the climatological average (Fig. 4b). The ice growth from frazil ice formation and ice growth in leads remained close to the climatological averages (Figs. 4c,d). The combined effect was a halt to the net growth of ice in the northeastern Barents Sea throughout February because of anomalous melting. The contribution from ice melting

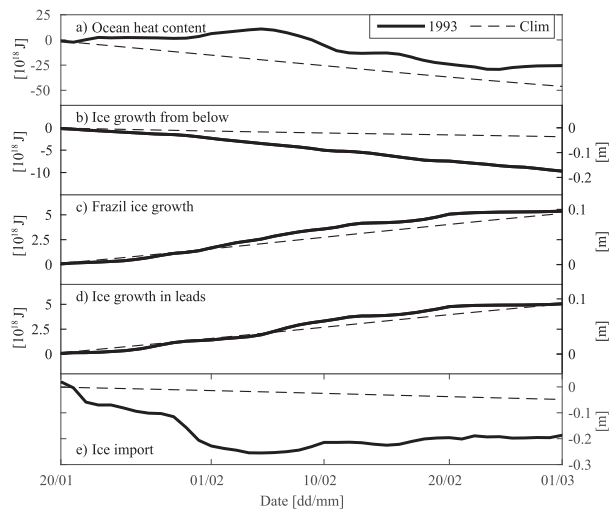


FIG. 4. (a) Cumulative daily change in ocean heat content within the box area (shaded box; Fig. 1). Thick black line denotes conditions in 1993. Dashed line denotes climatological conditions (1960–2014 average) based on monthly averages interpolated to daily averages. (b) As in (a), but for cumulative ice growth from below (positive = freezing). (c) As in (a), but for cumulative frazil ice growth. (d) As in (a), but for cumulative ice growth in leads. (e) As in (a), but for net ice advection through the boundaries of the box (positive is import into the box).

from the top was negligible. Furthermore, the wind conditions during the event of elevated wind stress curl caused an initial anomalous net sea ice export from the box accounting for almost 0.25 m (Fig. 4f). The positive sea ice anomaly southeast of Spitsbergen (Figs. 2d,e) is consistent with ice advection due to the anomalous northerly winds in the northwestern Barents Sea in February 1993 (Fig. 2c). After the initial export of sea ice out of the box, the anomalous ocean heat content prevented the exported sea ice to be replaced by net freezing throughout February.

The negative anomaly in the sea ice concentration seen in both observations and the model (Figs. 2d,e) allowed for a larger than normal heat loss to the atmosphere through surface heat fluxes (Fig. 2f). The monthly averaged net surface heat loss, as computed from the model heat budget within the box, exceeded 200 W m^{-2} in February (not shown). This represents an anomaly of 100 W m^{-2} relative to the climatological mean of $\sim 100 \text{ W m}^{-2}$ in February, in agreement with the heat flux anomaly in the northeastern Barents Sea in the atmospheric reanalysis (Fig. 2f).

To quantify the frequency of occurrence for events similar to the event described above, we extend our study to include the whole ocean model archive of 1960–2014. We focus on strong signals, defined as anomalies simultaneously exceeding 1.96 standard

deviations (corresponding to a confidence level of 95%), detectable in monthly averaged heat transport anomalies through the Barents Sea Opening and into the box. Furthermore, we use coherent (i.e., simultaneous) heat transport anomalies as a proxy for conditions favorable for the event described above. We then find a tendency of increased frequency of occurrence in the 1990s and onward compared with the preceding decades (Fig. 5). Out of a total of 16 occurrences, 5 happened during the 30 years prior to 1990 compared with 11 during the following 25 years. If we reduce the threshold to 1.65 standard deviations (corresponding to a confidence level of 90%), then 19 out of 33 events occurred after 1990.

5. Discussion

We have shown that positive wind stress curl and associated Ekman divergence in the Barents Sea causes a coherent increase in the Atlantic water heat transport. The immediate response connected to the associated local winds is a decrease in the sea ice cover due to advection in the northeastern Barents Sea. Despite the subsequent anomalous ocean-to-air heat loss due to the open water, the increase in the ocean heat content caused by the circulation anomaly reduced refreezing on a time scale of order one month.

In terms of the immediate sea ice response to wind forcing, our results agree with Kimura and Wakatsuchi (2001). Wind-driven ice advection is certainly a mechanism in effect that applies both to on- and off-ice wind conditions. However, for these winds to generate ocean heat transport anomalies, they need to be part of a larger-scale atmospheric field causing an anomalous Atlantic flow through the Barents Sea (Ingvaldsen et al. 2004; Skagseth et al. 2011; Lien et al. 2013a). A regional dependence has also been found in the strengths of the two branches of Atlantic water flow toward the Arctic through the Fram Strait (Chafik et al. 2015) and the Barents Sea (Lien et al. 2013a). Thus, the regional wind field over the Barents Sea area induces a mode of variability on time scales of about one month affecting changes in ocean circulation and sea ice, as well as ocean-to-air heat exchange.

Climate variability in the Barents Sea on annual and longer time scales has been linked to changes in temperature of the inflowing Atlantic water (Helland Hansen and Nansen 1909). Anomalies of heat transport modulated by changes in temperature [i.e., $Q(\bar{V}, T')$] in the Nordic and Barents Seas can either be formed locally or regionally through changes in air–sea heat fluxes (Schlichtholz 2013; Furevik 2000), or advected northward from the North Atlantic (Furevik 2001; Sandø

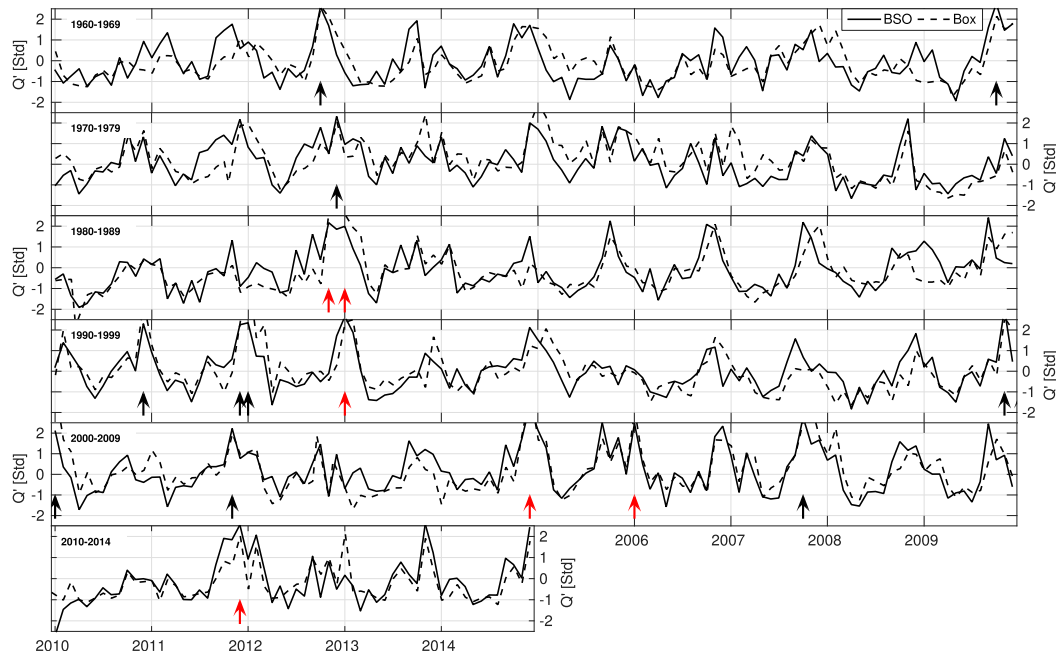


FIG. 5. Normalized monthly heat transport anomalies, relative to 1960–2014 average, through the Barents Sea Opening section (solid lines) and heat convergence anomaly in the box area (dashed lines). Arrows indicate months when both anomalies exceed 1.96 std dev (corresponding to 95% confidence). Red (blue) arrows denote months with normalized NAO above (below) 1. Black arrows denote months with NAO within one std dev from the mean. The temperature was detrended before the heat transports were calculated.

et al. 2010; Nakanowatari et al. 2014; Årthun and Eldevik 2016). The advective nature and annual time scales of these temperature anomalies enable predictability of the downstream sea ice cover (Årthun et al. 2012; Onarheim et al. 2015). Hence, also accounting for the regional mode of Barents Sea variability documented here and by others (Lien et al. 2013a; Chafik et al. 2015) might further improve the precision of seasonal-scale sea ice predictions.

We find that atmospherically driven coherent heat transport anomalies through the Barents Sea are a significant feature of the regional climate variability. Considering the whole simulation period (1960–2014) the occurrences of similar events have increased after 1990 (Fig. 5). Although the mechanism modulating Barents Sea ocean transport anomalies is forced regionally (Ingvaldsen et al. 2004; Skagseth et al. 2011; Lien et al. 2013a; Chafik et al. 2015), a positive NAO means a northward shift of the storm tracks in the Nordic seas and also an increase in the number of low pressure systems within the Nordic seas (e.g., Bader et al. 2011). This may also increase the number of atmospheric cyclones that enters the Barents Sea region, generating barotropic transport anomalies. Indeed, we find that 6 out of a total 16 months with the discussed coherent heat transport anomalies through the

Barents Sea occurred in months with normalized NAO above 1 and 15 out of 16, if only requiring a positive NAO. No such anomalies were found during months with NAO below -1 (Fig. 5). Since the events of reduced sea ice cover identified here are connected to a positive NAO state, they differ from the proposed teleconnections between increased Barents Sea heat fluxes and cold winters in midlatitudes associated with a negative NAO (e.g., Petoukhov and Semenov 2010). Rather, the mechanism investigated here in detail supports the hypothesis of a positive feedback loop where increased surface heat fluxes cause enhanced cyclonic activity favorable for increased Barents Sea inflow (Ikeda 1990; Ådlandsvik and Loeng 1991; Bengtsson et al. 2004). This is as opposed to the nonconclusive findings by Smedsrud et al. (2013), which were based on investigations at coarser spatio-temporal resolution.

Acknowledgments. This work has been supported by the joint Polish–Norwegian research project PAVE, Grant 202006. The authors thank Randi B. Ingvaldsen and Bjørn Ådlandsvik for fruitful discussions and three anonymous reviewers for comments and suggestions that helped improve the manuscript. We also thank Karen Gjertsen for the help in preparing Fig. 1.

REFERENCES

- Aagaard, K., and P. Greisman, 1975: Toward new mass and heat budgets for the Arctic Ocean. *J. Geophys. Res.*, **80**, 3821–3827, doi:10.1029/JC080i027p03821.
- ACIA, 2005: *Arctic Climate Impact Assessment*. Cambridge University Press, 1042 pp.
- Ådlandsvik, B., and H. Loeng, 1991: A study of the climatic system in the Barents Sea. *Polar Res.*, **10**, 45–49, doi:10.1111/j.1751-8369.1991.tb00633.x.
- Årthun, M., and T. Eldevik, 2016: On anomalous ocean heat transport toward the Arctic and associated climate predictability. *J. Climate*, **29**, 689–704, doi:10.1175/JCLI-D-15-0448.1.
- , —, L. H. Smedsrud, Ø. Skagseth, and R. B. Ingvaldsen, 2012: Quantifying the influence of Atlantic heat on Barents Sea ice variability and retreat. *J. Climate*, **25**, 4736–4743, doi:10.1175/JCLI-D-11-00466.1.
- Bader, J., M. D. S. Mesquita, K. I. Hodges, N. Keenlyside, S. Østerhus, and M. Miles, 2011: A review on Northern Hemisphere sea-ice, storminess and the North Atlantic Oscillation: Observations and projected changes. *Atmos. Res.*, **101**, 809–834, doi:10.1016/j.atmosres.2011.04.007.
- Bengtsson, L., V. A. Semenov, and O. M. Johannessen, 2004: The early twentieth-century warming in the Arctic—A possible mechanism. *J. Climate*, **17**, 4045–4057, doi:10.1175/1520-0442(2004)017<4045:TETWIT>2.0.CO;2.
- Budgell, W. P., 2005: Numerical simulation of ice–ocean variability in the Barents Sea region: Towards dynamical downscaling. *Ocean Dyn.*, **55**, 370–387, doi:10.1007/s10236-005-0008-3.
- Carton, J. A., and B. S. Giese, 2008: A reanalysis of ocean climate using Simple Ocean Data Assimilation (SODA). *Mon. Wea. Rev.*, **136**, 2999–3017, doi:10.1175/2007MWR1978.1.
- , G. Chepurin, X. Cao, and B. S. Giese, 2000: A Simple Ocean Data Assimilation analysis of the global upper ocean 1950–95. Part I: Methodology. *J. Phys. Oceanogr.*, **30**, 294–309, doi:10.1175/1520-0485(2000)030<0294:ASODAA>2.0.CO;2.
- Cavalieri, D., C. Parkinson, P. Gloersen, and H. J. Zwally, 1996: Sea ice concentrations from Nimbus-7 SMMR and DMSP SSM/I-SSMIS passive microwave data. National Snow and Ice Data Center, accessed June 2015. [Available online at www.nsidc.org/data/NSIDC-0051.]
- Chafik, L., J. Nilsson, Ø. Skagseth, and P. Lundberg, 2015: On the flow of Atlantic water and temperature anomalies in the Nordic seas toward the Arctic Ocean. *J. Geophys. Res.*, **120**, 7897–7918, doi:10.1002/2015JC011012.
- Chapman, D. C., 1985: Numerical treatment of cross-shelf open boundaries in a barotropic coastal ocean model. *J. Phys. Oceanogr.*, **15**, 1060–1075, doi:10.1175/1520-0485(1985)015<1060:NTOCSO>2.0.CO;2.
- Cohen, J., and Coauthors, 2014: Recent Arctic amplification and extreme mid-latitude weather. *Nat. Geosci.*, **7**, 627–637, doi:10.1038/ngeo2234.
- Comiso, J. C., 2012: Large decadal decline of the Arctic multiyear ice cover. *J. Climate*, **25**, 1176–1193, doi:10.1175/JCLI-D-11-00113.1.
- Dee, D. P., and Coauthors, 2011: The ERA-Interim reanalysis: Configuration and performance of the data assimilation system. *Quart. J. Roy. Meteor. Soc.*, **137**, 553–597, doi:10.1002/qj.828.
- Flather, R. A., 1976: A tidal model of the northwest European continental shelf. *Mem. Soc. Roy. Sci. Liege*, **6**, 141–164.
- Fosheim, M., R. Primicerio, E. Johannessen, R. B. Ingvaldsen, M. M. Aschan, and A. V. Dolgov, 2015: Recent warming leads to a rapid borealization of fish communities in the Arctic. *Nat. Climate Change*, **5**, 673–677, doi:10.1038/nclimate2647.
- Frankignoul, C., N. Sennéchaël, and P. Cauchy, 2014: Observed atmospheric response to cold season sea ice variability in the Arctic. *J. Climate*, **27**, 1243–1254, doi:10.1175/JCLI-D-13-00189.1.
- Furevik, T., 2000: On anomalous sea surface temperatures in the Nordic seas. *J. Climate*, **13**, 1044–1053, doi:10.1175/1520-0442(2000)013<1044:OASSTI>2.0.CO;2.
- , 2001: Annual and interannual variability of Atlantic Water temperatures in the Norwegian and Barents Seas: 1980–1996. *Deep-Sea Res. I*, **48**, 383–404, doi:10.1016/S0967-0637(00)00050-9.
- Gill, A. E., and E. H. Schumann, 1974: The generation of long shelf waves by the wind. *J. Phys. Oceanogr.*, **4**, 83–90, doi:10.1175/1520-0485(1974)004<0083:TGOLSW>2.0.CO;2.
- Häkkinen, S., and G. L. Mellor, 1992: Modelling the seasonal variability of a coupled Arctic ice–ocean system. *J. Geophys. Res.*, **97**, 20 285–20 304, doi:10.1029/92JC02037.
- Helland-Hansen, B., and F. Nansen, 1909: *The Norwegian Sea: Its Physical Oceanography based upon the Norwegian Research 1900–1904*. Part 1, *Reports on Norwegian Fishery and Marine Investigations*, Det Mallingske Bogtrykkeri, 390 pp.
- Herbaut, C., M.-N. Houssais, S. Close, and A.-C. Blaizot, 2015: Two wind-driven modes of winter sea ice variability in the Barents Sea. *Deep-Sea Res. I*, **106**, 97–115, doi:10.1016/j.dsr.2015.10.005.
- Hunke, E., 2001: Viscous–plastic sea ice dynamics with the EVP model: Linearization issues. *J. Comput. Phys.*, **170**, 18–38, doi:10.1006/jcph.2001.6710.
- , and J. Dukowicz, 1997: An elastic–viscous–plastic model for sea ice dynamics. *J. Phys. Oceanogr.*, **27**, 1849–1867, doi:10.1175/1520-0485(1997)027<1849:AEVPMF>2.0.CO;2.
- Hurrell, J. W., 1995: Decadal trends in the North Atlantic Oscillation: Regional temperatures and precipitation. *Science*, **269**, 676–679, doi:10.1126/science.269.5224.676.
- Ikeda, M., 1990: Decadal oscillations of the air–ice–ocean systems in the Northern Hemisphere. *Atmos.–Ocean*, **28**, 106–139, doi:10.1080/07055900.1990.9649369.
- Ingvaldsen, R., H. Loeng, and L. Asplin, 2002: Variability in the Atlantic inflow to the Barents Sea based on a one-year time series from moored current meters. *Cont. Shelf Res.*, **22**, 505–519, doi:10.1016/S0278-4343(01)00070-X.
- , L. Asplin, and H. Loeng, 2004: Velocity field of the western entrance to the Barents Sea. *J. Geophys. Res.*, **109**, C03021, doi:10.1029/2003JC001811.
- Johannessen, O. M., and Coauthors, 2004: Arctic climate change: Observed and modelled temperature and sea-ice variability. *Tellus*, **56A**, 328–341, doi:10.1111/j.1600-0870.2004.00060.x.
- Kalnay, E., and Coauthors, 1996: The NCEP/NCAR 40-Year Reanalysis Project. *Bull. Amer. Meteor. Soc.*, **77**, 437–470, doi:10.1175/1520-0477(1996)077<0437:TNYRP>2.0.CO;2.
- Kimura, N., and M. Wakatsuchi, 2001: Mechanisms for the variation of sea ice extent in the Northern Hemisphere. *J. Geophys. Res.*, **106**, 31 319–31 331, doi:10.1029/2000JC000739.
- Lien, V. S., Y. Gusdal, J. Albretsen, A. Melsom, and F. B. Vikebø, 2013a: *Evaluation of a Nordic seas 4 km Numerical Ocean Model Hindcast Archive (SVIM), 1961–2011*. Fisker og Havet 7, Havforskningsinstituttet, 79 pp.
- , F. B. Vikebø, and Ø. Skagseth, 2013b: One mechanism contributing to co-variability of the Atlantic inflow branches to the Arctic. *Nat. Commun.*, **4**, 1488, doi:10.1038/ncomms2505.
- , Y. Gusdal, and F. B. Vikebø, 2014: Along-shelf hydrographic anomalies in the Nordic seas (1960–2011): Locally generated or advective signals? *Ocean Dyn.*, **64**, 1047–1059, doi:10.1007/s10236-014-0736-3.
- , and Coauthors, 2016: An assessment of the added value from data assimilation on modelled Nordic seas hydrography and

- ocean transports. *Ocean Modell.*, **99**, 43–59, doi:[10.1016/j.ocemod.2015.12.010](https://doi.org/10.1016/j.ocemod.2015.12.010).
- Lind, S., and R. B. Ingvaldsen, 2012: Variability and impacts of Atlantic Water entering the Barents Sea from the north. *Deep-Sea Res. I*, **62**, 70–88, doi:[10.1016/j.dsr.2011.12.007](https://doi.org/10.1016/j.dsr.2011.12.007).
- Marchesiello, P., J. C. McWilliams, and A. Shchepetkin, 2001: Open boundary conditions for long-term integration of regional oceanic models. *Ocean Modell.*, **3**, 1–20, doi:[10.1016/S1463-5003\(00\)00013-5](https://doi.org/10.1016/S1463-5003(00)00013-5).
- Mellor, G. L., and L. Kantha, 1989: An ice–ocean coupled model. *J. Geophys. Res.*, **94**, 10 937–10 954, doi:[10.1029/JC094iC08p10937](https://doi.org/10.1029/JC094iC08p10937).
- , M. G. McPhee, and M. Steele, 1986: Ice seawater turbulent boundary layer interaction with melting or freezing. *J. Phys. Oceanogr.*, **16**, 1829–1846, doi:[10.1175/1520-0485\(1986\)016<1829:ISTBLI>2.0.CO;2](https://doi.org/10.1175/1520-0485(1986)016<1829:ISTBLI>2.0.CO;2).
- Mori, M., M. Watanabe, H. Shioyama, J. Inoue, and M. Kimoto, 2014: Robust Arctic sea-ice influence on the frequent Eurasian cold winters in past decades. *Nat. Geosci.*, **7**, 869–873, doi:[10.1038/ngeo2277](https://doi.org/10.1038/ngeo2277).
- Nakanowatari, T., K. Sato, and J. Inoue, 2014: Predictability of the Barents Sea ice in early winter: Remote effects of oceanic and atmospheric thermal conditions from the North Atlantic. *J. Climate*, **27**, 8884–8901, doi:[10.1175/JCLI-D-14-00125.1](https://doi.org/10.1175/JCLI-D-14-00125.1).
- Onarheim, I. H., T. Eldevik, M. Årthun, R. B. Ingvaldsen, and L. H. Smedsrud, 2015: Skillful prediction of Barents Sea ice cover. *Geophys. Res. Lett.*, **42**, 5364–5371, doi:[10.1002/2015GL064359](https://doi.org/10.1002/2015GL064359).
- Ozhigin, V., R. B. Ingvaldsen, H. Loeng, V. Boitsov, and A. Karsakov, 2011: Introduction to the Barents Sea. *The Barents Sea: Ecosystem, Resources, Management: Half a Century of Russian–Norwegian Cooperation*. T. Jakobsen and V. Ozhigin, Eds., Tapir Academic Press, 39–76.
- Parkinson, C. L., and D. J. Cavalieri, 2012: Arctic sea ice variability and trends, 1979–2010. *The Cryosphere Discuss.*, **6**, 871–880, doi:[10.5194/tcd-6-931-2012](https://doi.org/10.5194/tcd-6-931-2012).
- Pavlova, O., V. Pavlov, and S. Gerland, 2014: The impacts of winds and sea surface temperatures on the Barents Sea ice extent, a statistical approach. *J. Mar. Syst.*, **130**, 248–255, doi:[10.1016/j.jmarsys.2013.02.011](https://doi.org/10.1016/j.jmarsys.2013.02.011).
- Petoukhov, V., and V. A. Semenov, 2010: A link between reduced Barents–Kara Sea ice and cold winter extremes over northern continents. *J. Geophys. Res.*, **115**, D21111, doi:[10.1029/2009JD013568](https://doi.org/10.1029/2009JD013568).
- Polyakov, I. V., and Coauthors, 2010: Arctic Ocean warming contributes to reduced polar ice cap. *J. Phys. Oceanogr.*, **40**, 2743–2756, doi:[10.1175/2010JPO4339.1](https://doi.org/10.1175/2010JPO4339.1).
- Reistad, M., Ø. Breivik, H. Haakenstad, O. J. Aarnes, B. R. Furevik, and J. R. Bidlot, 2011: A high-resolution hindcast of wind and waves for the North Sea, the Norwegian Sea, and the Barents Sea. *J. Geophys. Res.*, **116**, C05019, doi:[10.1029/2010JC006402](https://doi.org/10.1029/2010JC006402).
- Sandø, A. B., J. E. Ø. Nilsen, Y. Gao, and K. Lohmann, 2010: Importance of heat transport and local air–sea heat fluxes for Barents Sea climate variability. *J. Geophys. Res.*, **115**, C07013, doi:[10.1029/2009JC005884](https://doi.org/10.1029/2009JC005884).
- , —, T. Eldevik, and M. Bentsen, 2012: Mechanisms for variable North Atlantic–Nordic seas exchanges. *J. Geophys. Res.*, **117**, C12006, doi:[10.1029/2012JC008177](https://doi.org/10.1029/2012JC008177).
- Schlichtholz, P., 2011: Influence of oceanic heat variability on sea ice anomalies in the Nordic seas. *Geophys. Res. Lett.*, **38**, L05705, doi:[10.1029/2010GL045894](https://doi.org/10.1029/2010GL045894).
- , 2013: Observational evidence for oceanic forcing of atmospheric variability in the Nordic seas area. *J. Climate*, **26**, 2957–2975, doi:[10.1175/JCLI-D-11-00594.1](https://doi.org/10.1175/JCLI-D-11-00594.1).
- , 2014: Local wintertime tropospheric response to oceanic heat anomalies in the Nordic seas area. *J. Climate*, **27**, 8686–8706, doi:[10.1175/JCLI-D-13-00763.1](https://doi.org/10.1175/JCLI-D-13-00763.1).
- , 2016: Empirical relationships between summertime oceanic heat anomalies in the Nordic seas and large-scale atmospheric circulation in the following winter. *Climate Dyn.*, **47**, 1735–1753, doi:[10.1007/s00382-015-2930-5](https://doi.org/10.1007/s00382-015-2930-5).
- Screen, J. A., and I. Simmonds, 2010: Increasing fall–winter energy loss from the Arctic Ocean and its role in Arctic temperature amplification. *Geophys. Res. Lett.*, **37**, L16707, doi:[10.1029/2010GL044136](https://doi.org/10.1029/2010GL044136).
- , —, C. Deser, and R. Tomas, 2013: The atmospheric response to three decades of observed Arctic sea ice loss. *J. Climate*, **26**, 1230–1248, doi:[10.1175/JCLI-D-12-00063.1](https://doi.org/10.1175/JCLI-D-12-00063.1).
- Serreze, M. C., M. M. Holland, and J. C. Stroeve, 2007: Perspectives on the Arctic’s shrinking sea-ice cover. *Science*, **315**, 1533–1536, doi:[10.1126/science.1139426](https://doi.org/10.1126/science.1139426).
- Shchepetkin, A. F., and J. C. McWilliams, 2005: The Regional Ocean Modeling System (ROMS): A split-explicit, free-surface, topography-following coordinates ocean model. *Ocean Modell.*, **9**, 347–404, doi:[10.1016/j.ocemod.2004.08.002](https://doi.org/10.1016/j.ocemod.2004.08.002).
- Skagseth, Ø., K. Drinkwater, and E. Terrile, 2011: Wind and buoyancy induced transport of the Norwegian Coastal Current in the Barents Sea. *J. Geophys. Res.*, **116**, C08007, doi:[10.1029/2011JC006996](https://doi.org/10.1029/2011JC006996).
- Smedsrud, L. H., and Coauthors, 2013: The role of the Barents Sea in the climate system. *Rev. Geophys.*, **51**, 415–449, doi:[10.1002/rog.20017](https://doi.org/10.1002/rog.20017).
- Sorokina, S. A., C. Li, J. J. Wettstein, and N. G. Kvamstø, 2016: Observed atmospheric coupling between Barents Sea ice and the warm-Arctic cold-Siberian anomaly pattern. *J. Climate*, **29**, 495–511, doi:[10.1175/JCLI-D-15-0046.1](https://doi.org/10.1175/JCLI-D-15-0046.1).
- Sorteberg, A., and B. Kvingedal, 2006: Atmospheric forcing on the Barents Sea winter ice extent. *J. Climate*, **19**, 4772–4784, doi:[10.1175/JCLI3885.1](https://doi.org/10.1175/JCLI3885.1).
- Sundby, S., and K. Drinkwater, 2007: On the mechanisms behind salinity anomaly signals of the northern North Atlantic. *Prog. Oceanogr.*, **73**, 190–202, doi:[10.1016/j.pocean.2007.02.002](https://doi.org/10.1016/j.pocean.2007.02.002).
- Umlauf, L., and H. Burchard, 2003: A generic length-scale equation for geophysical turbulence models. *J. Mar. Res.*, **61**, 235–265, doi:[10.1357/002224003322005087](https://doi.org/10.1357/002224003322005087).
- , —, and K. Hutter, 2003: Extending the $k-\omega$ turbulence model towards oceanic applications. *Ocean Modell.*, **5**, 195–218, doi:[10.1016/S1463-5003\(02\)00039-2](https://doi.org/10.1016/S1463-5003(02)00039-2).
- Varpe, Ø., M. Daase, and T. Kristiansen, 2015: A fish-eye view on the new Arctic lightscape. *ICES J. Mar. Sci.*, **72**, 2532–2538, doi:[10.1093/icesjms/fsv129](https://doi.org/10.1093/icesjms/fsv129).
- Vihma, T., 2014: Effects of Arctic sea ice decline on weather and climate: A review. *Surv. Geophys.*, **35**, 1175–1214, doi:[10.1007/s10712-014-9284-0](https://doi.org/10.1007/s10712-014-9284-0).
- Warner, J. C., and W. R. Geyer, 2005: Numerical modelling of an estuary: A comprehensive skill assessment. *J. Geophys. Res.*, **110**, C055001, doi:[10.1029/2004JC002691](https://doi.org/10.1029/2004JC002691).
- , C. R. Sherwood, H. G. Arango, and R. P. Signell, 2005: Performance of four turbulence closure methods implemented using a generic length scale method. *Ocean Modell.*, **8**, 81–113, doi:[10.1016/j.ocemod.2003.12.003](https://doi.org/10.1016/j.ocemod.2003.12.003).
- Yang, X.-Y., X. Yuan, and M. Ting, 2016: Dynamical link between the Barents–Kara Sea ice and the Arctic Oscillation. *J. Climate*, **29**, 5103–5122, doi:[10.1175/JCLI-D-15-0669.1](https://doi.org/10.1175/JCLI-D-15-0669.1).